Nanoscale Rheology and Anisotropic Diffusion Using Single Gold Nanorod Probes

Mehdi Molaei, Ehsan Atefi, and John C. Crocker

Nanoscale Rheology and Anisotropic Diffusion

using Single Gold Nanorod Probes

Mehdi Molaei, Ehsan Atefi, John C. Crocker*

Chemical and Biomolecular Engineering, University of Pennsylvania,

220 S. 33rd St, Philadelphia, PA 19104

The complex rotational and translational Brownian motion of anisotropic particles depends on their shape and the viscoelasticity of their surroundings. Due to their strong optical scattering and chemical versatility, gold nanorods would seem to provide the ultimate probes of rheology at the nanoscale, but the suitably accurate orientational tracking required to compute rheology has not been demonstrated. Here we image single gold nanorods with a laser-illuminated dark-field microscope, and use optical polarization to determine their three-dimensional orientation to better than one degree. We convert the rotational diffusion of single nanorods in viscoelastic polyethylene glycol solutions to rheology, and obtain excellent agreement with bulk measurements. Extensions of earlier models of anisotropic translational diffusion to three dimensions and viscoelastic fluids give excellent agreement with the observed motion of single nanorods. We find that nanorod tracking provides a uniquely capable approach to microrheology, and provides a powerful tool for probing nanoscale dynamics and structure in a range of soft materials.

The Brownian motion of embedded tracers has been applied to determining the viscoelasticity of soft materials and microscopic objects via passive microrheology for more than two decades. Typically, dynamic light scattering [1-4] or image-based particle tracking [3,5-9] is used to measure the tracers' mean squared displacement (MSD) which is then converted to the dynamic shear modulus via a generalized Stoke-Einstein relation (GSER) [1,2,4,10]. Pioneering work by Cheng and Mason [11] showed that the rotational diffusion of anisotropic micron-scale particles can also be used to quantify the rheology via a rotational GSER, and later was demonstrated using depolarized dynamic light scattering [12,13]. Multiple imaging-based rotational tracking methods have since been reported [14-18], however, they do not appear well-suited to microrheology. While the use of anisotropic nanoparticle tracers would greatly facilitate the application of this approach to stiffer materials and much smaller length and time scales than possible with larger tracers, microrheology places stringent requirements on the accuracy of the tracer's inferred mean-squared displacement. Indeed, despite several reports of gold nanorod (GNR) rotational tracking using imaging [19-31] and depolarized scattering [32-36], no one has demonstrated the use of GNRs to accurately measure the rheology of a viscoelastic material. Moreover, no models of the complex anisotropic translational diffusion [32,33,37] that these particles would execute in a viscoelastic material, or its coupling to the rotational diffusion, have been reported or validated.

Here, we study the rotational and translational Brownian motion of single gold nanorods (GNRs) using a laser-illuminated dark-field microscope modified to simultaneously record two orthogonally polarized images. A polarimetric analysis, based upon a nano-optical model of the GNR, enables the accurate determination of the rods' three-dimensional orientation to better than one degree at up to several thousand frames per second. The rotational diffusion motion quantified by a mean-squared angular displacement can be quantitatively converted into a dynamic shear modulus via a generalized Stokes-Einstein relation. We demonstrate this 'nanorheology' approach in concentrated viscoelastic solutions of polyethylene glycol polymer; extending passive microrheology down to 100 nm length and single attoliter (10^{-18} l) volume scales. Moreover, we extend an earlier study [37] of two-dimensional anisotropic translational

diffusion [38] in Newtonian fluids to the unbounded, three-dimensional and the viscoelastic cases, and find that it accurately reproduces the observed motion of single isolated nanorods.

GNRs are ideal orientation probes since their surface plasmon resonance [22], depends on their relative orientation with respect to the external electric field [39] and their scattered light is thus strongly polarized [26,40]. Previous studies [26,39,40] have shown that far-field scattered light of a single GNR can be modeled by the electric field emitted from three independent and orthogonal principal dipoles, with the dipole aligned along the rod's long axis being predominant. We computed the strength of these principal dipoles using the discrete dipole approximation (DDA) method [41-44], (see SI.1 for details [45]). We image the particles using a custom-built dark-field microscope that focuses a single mode, 300 mW diode pumped solid state (DPSS) laser (λ=670nm) in the back-aperture of a high-NA, oil-immersion objective to produce a small, collimated Gaussian beam in the specimen, Fig. 1a. We took advantage of the polarization sensitivity of GNR scattering by illuminating the rod with a circularly polarized laser beam, and splitting the scattered light into two images on the same camera detector, corresponding to two orthogonal linear polarization channels [45]. The integrated intensity of the GNR images in these two channels is a function of the GNRs orientation, specifically, its polar angle, β, and azimuthal angle, ϕ, Fig. 1c. We use a semi-analytic physical optics model to compute the expected intensities in our high numerical aperture microscope. Inverting these periodic functions maps the inferred position of the rod's orientation into a single octant domain of the unit sphere. While this precludes determining the absolute spatial orientation of the rod, it does allow the angular mean-squared displacement, needed for microrheology, to be reliably determined.
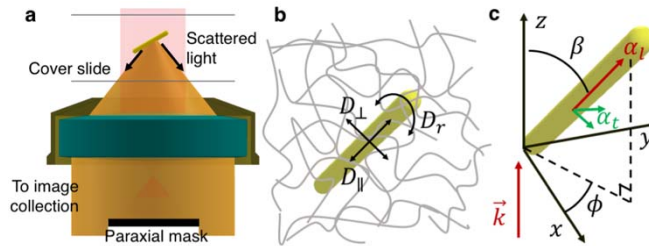

FIG. 1. a) Gold nanorod (GNR) scattering and imaged by a dark-field microscope. b) GNR embedded in viscoelastic polymer solution c) Coordinate system of the GNR defined by polar, β, and azimuthal angles, ϕ.
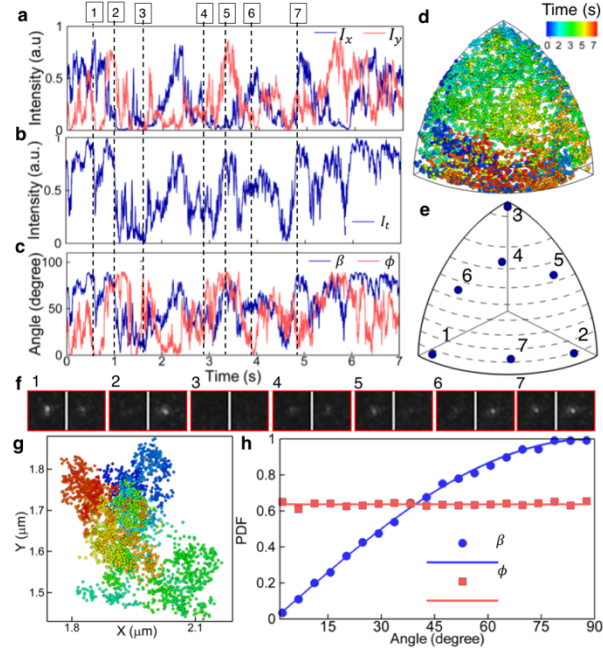
FIG. 2. Integrated intensity of a GNR in glycerol in orthogonal x, and y polarization images (a); with the corresponding sum of intensities (b) and the inferred orientation angles (c). Time dependent 3D GNR orientation mapped into a single octant (d). Orientations of selected time points (1-7) marked in (e); corresponding image pairs (1.6×1.6 μm²) in (f). Trajectory (g) of the GNR showing translational motion. Frequency distributions of orientation angles (h) from 10^5 image pairs (symbols) match a random orientation model (curves).

To demonstrate the angular tracking capability of the imaging system, we first studied the motion of GNRs (20×100 nm²) in pure glycerol. The intensity of the scattering light in the x and y channels and the total intensity are shown as functions of time in Fig. 2a-b. Fig. 2c shows the inferred polar and azimuthal angles of a single GNR versus time. As expected, the inferred GNR orientation, as shown in Fig. 2d, fully explores the available octant of a unit sphere. Typical images of the GNR at different orientations at selected times, are shown in Fig. 2f. Tracking the centroid position of the GNR over time, Fig. 2g, indicates that translational Brownian motion of the GNR is small enough that rods do not go out of focus during image collection. The shape of the distribution of polar angles and azimuthal angles, over 10^5 image pairs is consistent with the GNR exploring all orientations randomly to within statistical sampling, Fig. 2h, confirming the accuracy of our polarimetric analysis.

4

The mean-squared angular displacement (MSAD), $MSAD = \langle|u(t+\tau) - u(t)|^2\rangle_t$, is bounded by the direction vector being limited to the unit sphere, leading to a single exponential cross-over with an asymptote of 2, $\langle-\Delta\hat{u}^2(t)\rangle = 2[1 - (1 - \varepsilon_r^2)\exp(-2D_r t)]$, where D_r is the rotational diffusion coefficient, and ε_r is the measurement error in the orientation vector [14,53,54], (Fig. S5a). With unit vectors mapped to an octant a similar effect occurs; Monte Carlo (MC) simulations [45] show that the resulting MSAD is well described empirically by a stretched exponential function with an asymptote of 0.5:

$$\langle|\Delta\hat{u}^2(t)|\rangle = \frac{1}{2}\left[1 - (1 - \varepsilon_r^2)\exp(-(\kappa D_r t)^\zeta)\right] \tag{1}$$

where $\kappa = 1.6$ and $\zeta = 0.95$ are constants (Fig. 3a). Equation 1 compares favorably to the MSAD determined for single GNRs in pure glycerol, (Fig. 3b). Fitting yields a rotational diffusion constant $D_r = 3.5\ rad^2/s$, and an estimated angular measurement uncertainty $\varepsilon_r^2 = 2.5 \times 10^{-4}\ rad^2$, better than 1° directional precision. We also determined the translational diffusion coefficient by fitting to the short lag time data from centroid-based particle tracking [53] (Fig. S5c), $\langle\Delta r_{xy}^2\rangle = 4D_t t + 4\varepsilon_t^2$. This yields a value of $D_t = 0.007\ \mu m^2/s$ and a position uncertainty of ~9 nm.

The theoretical prediction of translational and rotational diffusion coefficients for a rod (in the lab frame), are $D_r = \frac{3KT}{\pi\eta l^3}[\ln\rho + C_r(\rho)]$ and $D_t = \frac{KT}{3\pi\eta l}[\ln\rho + C_t(\rho)]$, where K and T are Boltzmann constant and temperature, l and d are the length and diameter of the rod, and C_r and C_t are the rotational and translational drag coefficient correction factors which are function of aspect ratio, ρ, and the shape of the rod ends [18,55,56]. The ratio of the translational to the rotational diffusion coefficients is only a function of the geometry of the GNR, $\frac{D_t}{D_r} = l^2 f(\rho)$. Electron microscopy shows that the rods have a consistent 20nm diameter and lengths of 100±11nm, data shown in SI [45]. Using a spherocylinder model, and assuming the rods are stripped of their CTAB ligands in neat glycerol, the length of the single GNR tracer is inferred to be $l = 107\pm2\ nm$. and the viscosity of the solution can be estimated as $\eta = 1.26\ Pa.s$, in excellent agreement with the expected value of 1.29 Pa.s, for pure glycerol at 21±1.5 °C.
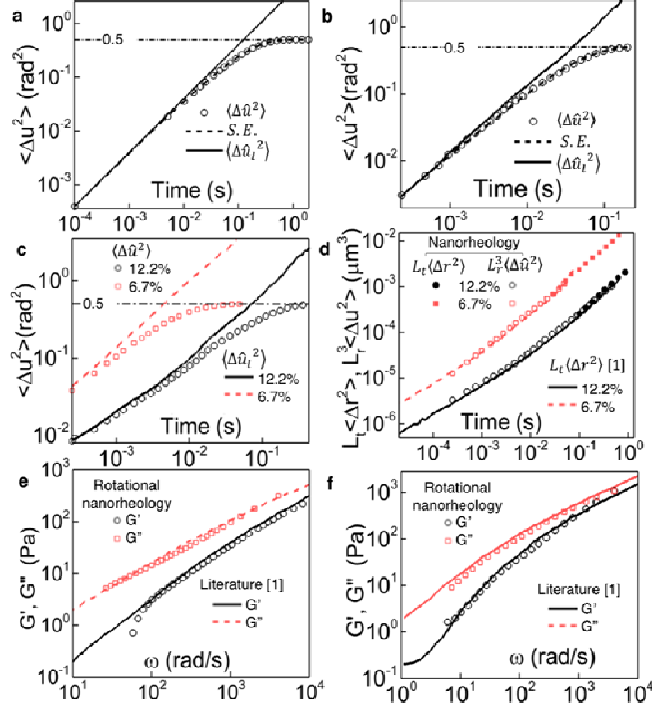
FIG. 3. MSADs of simulated (a) and measured (b) GNR in glycerol, (circles), stretched exponential fit (dashed line), and unbounded MSAD (curve). Measured MSADs (c) of a GNR in 200 kDa PEO, 6.7 % w/w (squares) and 12.2 % w/w (circles). (d) Scaled unbound MSAD (open symbols), translational MSD (closed circles) of the GNR and rescaled microsphere MSD [1](lines) at two PEO concentrations. Storage and loss moduli for PEO solution obtained from GNR rotational nanorheology (symbols) and literature microrheology [1] (lines) at 6.7% w/w (e) and 12.2% w/w (f).

The rotational diffusion of a nanorod in a viscoelastic material has been described by a Langevin torque equation   where   is the angular velocity of the nanorod,   is the thermal driving torque, and   is the rotational memory function [11]. Mason *et al*. have shown that the solution of this equation is similar to that for the translational Langevin equation [3]. Taking the Laplace transform of the Langevin equation, applying the principles of causality and thermal energy equipartition, and neglecting the inertia term, the Laplace transform of the angular velocity will be   . Taking the GNR as a spherocylinder leads to the Laplace transform of the rotational memory function to be   –   where   is the frequency dependent viscosity. Replacing   with —   leads to the rotational generalized Stokes Einstein relation (RGSER) for the GNR

$$\overline{}$$ (2)

where $\Delta\tilde{u}_l^2(s)$ is the Laplace transform of an MSAD, $\langle\Delta\hat{u}_l^2(t)\rangle$, that unlike $\langle\Delta\hat{u}^2(t)\rangle$ is unbounded in magnitude at long lag time. We developed an approach that computes a lag-time independent mapping between these two bounded and unbounded MSADs by inverting Eq. 1, which leads to $\langle\Delta\hat{u}_l^2(t)\rangle = 4D_r t = \frac{4}{k}\left[\ln\frac{1}{1-2\langle\Delta\hat{u}^2(t)\rangle}\right]^{1/\zeta}$. We validated this procedure using simulated trajectories of tracer beads in different model viscoelastic fluids using a method developed by Khan and Mason [50], see SI.7 [45]. This procedure has the expected effect of linearizing the bounded MSAD of GNR in the glycerol solution, see Fig. 3b. A limitation of this approach is the amplification of uncertainties in $\langle\Delta\hat{u}^2(t)\rangle$ for lag times longer than the rod's Brownian tumbling time, which limits the usefulness of this method as the bounded MSAD approaches its asymptotic values.

To demonstrate the feasibility of using Eq. 2 to measure non-diffusive Brownian motion and viscoelasticity with single GNRs, we suspended rods in an aqueous polyethylene oxide (PEO) solution (200 K molecular weight, 6.7% and 12.2% w/w), previously employed in a microrheology study by Dasgupta *et al.* [1]. In both samples the diameter of the rods is larger than the mesh sizes of the entangled polymer solutions at these concentrations (See SI for more detail of polymer characteristics [45]). Measured bounded MSAD, shown by symbols in Fig. 3c were remapped to unbounded MSADs, shown in Fig. 3c by lines.

To validate our tracking results, we can compare them to those of the earlier microsphere study using the same viscoelastic sample, by rescaling the MSDs as $L_t\langle\Delta\tilde{r}^2(s)\rangle$ and MSADs with $L_r^3\langle\Delta\tilde{u}_l^2(s)\rangle$, where L_t and L_r are translational and rotational effective length of probes derived from equating $\tilde{G}(s) = s\tilde{\eta}(s) = \frac{2k_B T}{\pi s L_r^3\langle\Delta\tilde{u}_l^2(s)\rangle} = \frac{2k_B T}{\pi s L_t\langle\Delta\tilde{r}^2(s)\rangle}$. For a sphere of diameter d, $L_t = L_r = d$, and for a nanorod with length of l and aspect ratio of ρ, $L_t = \frac{l}{(\ln\rho + C_t)}$ and $L_r = \frac{l}{\sqrt[3]{\ln\rho + C_r}}$. The $L_r^3\langle\Delta\hat{u}_l^2\rangle$ and $L_t\langle\Delta r^2\rangle$ of our single GNRs in the two PEO solutions is shown with open and closed symbols respectively in Fig. 3d. As in glycerol, the length of the GNRs in the 6.7% and 12.2% w/w PEO solution samples are determined by aligning the scaled MSDs and MSADs of the GNRs to be l=94±2 nm in 6.7% sample and l=101±2nm in 12.2% respectively. Our results compare favorably with $L_t\langle\Delta r^2\rangle$ of 0.65 µm diameter microspheres, deduced from the previous microrheology study [1] differing

7

systematically by about 15%. Because excess CTAB was added to the PEO solution, we assume that the CTAB layers are intact, and that the effective rod diameter, 26 nm, is correspondingly larger than seen using EM.

Small deviations of the GNR data are attributable to two main sources: the aforementioned noise amplification of our mapping procedure at long times and dynamic error which occurs at short times [53,54], which can be empirically corrected by considering results at different camera exposure time [45]. Physically, our rod motion may deviate from the predictions of the Stokes-Einstein relation due to polymer depletion near the rod surface [5,57] or decoupling from the bulk dynamics of the polymer solution [58-61], but both effects are expected to be small in our system.

As with conventional passive microrheology [1], we used a Fourier representation of the RGSER $G^*(\omega) = \frac{k_B T}{\pi s L_r^3 \mathcal{F}\{\langle \Delta \hat{u}_l^2(t) \rangle\}}$ to compute the elastic $G'(\omega)$ and loss $G''(\omega)$ moduli, where $\mathcal{F}\{\langle \Delta \hat{u}_l^2(t) \rangle\}$ is the unilateral Fourier transform of the unbounded MSAD [1]. The elastic and shear moduli of the two PEO solutions obtained from single GNR rotational nanorheology, are shown in Fig. 3e-f by open symbols, compared to literature measurements based on diffusive wave spectroscopy [1], shown by lines. In both samples, the maximum frequency at which we can probe the viscoelasticity is limited by the maximum recording speed and the minimum exposure time of the camera, while the minimum frequency is set by the MSAD reaching its asymptote. Notably, considering the size of the measurement uncertainties we have obtained with 100 nm GNRs, the maximum modulus that can be measured by rotational nanorheology, $G^*_{max} \approx \frac{K_B T}{l^3 \Delta u_{min}^2}$, is two orders of magnitude larger than measurable using translational microrheology, $G^*_{max} \approx \frac{K_B T}{l \Delta r_{min}^2}$.

The anisotropic translational Brownian motion of the GNR can be characterized by two drag coefficients parallel and perpendicular to its long axis. Following the analysis of Han *et al.* [37], in the moving body frame of the rod, translational displacements, as shown in Fig. 4a, have a Gaussian distribution, and the corresponding MSDs in a viscous fluid, as plotted in Fig. 4b, are linear function of time $\langle \Delta r_{\parallel,\perp}^2 \rangle = 2D_{\parallel,\perp} t$, with $D_\parallel$ and $D_\perp$ being diffusion coefficients parallel and perpendicular to the major axis, Fig. 1b. In a stationary lab frame initially aligned with the rod at t=0, however, rotational diffusion of the GNR

erases the particles alignment with the reference frame, causing translational diffusion to become isotropic [37] for $\tau > \tau_\theta = 1/2D_r$. To capture the this effect, we decomposed the MSDs of single GNRs into x and y directions with initial orientation aligned in the x direction, $\langle \Delta r_{x,y}^2 \rangle_{\hat{u}(0)=\hat{e}_x}$, results shown in Fig. 4c. As expected initially, $D_{xx}(t < \tau_\theta)$ equals to $D_\parallel$, and $D_{yy}(t < \tau_\theta)$ equals to $D_\perp$, before asymptotically approaching $D_t = (D_\parallel + 2D_\perp)/3$ at long times.

To describe such an anisotropic-to-isotropic crossover of the diffusion of uniaxial particles we generalized the Perrin-Lubensky model [37,38] to three-dimensional rotation [45]. For a rod diffusing in a viscous fluid in 3D, we obtain:

$$D_{ii} = \frac{\langle \Delta r_i^2 \rangle_{\hat{u}(0)}}{2t} = D_t + \Delta D \left(u_i^2(0) - \frac{1}{3} \right) \frac{\tau}{t}, \tag{3}$$

where $\Delta D = D_\parallel - D_\perp$, and $\tau = (1 - \exp(-6D_r t))/6D_r$, in excellent agreement with the data, Fig. 4c. For an anisotropic particle such as GNR, the functional dependence of the translational drag coefficients on its orientation mixes correlation between translational and orientational degrees of freedom [37]. For example, we measured two cross-terms $\langle \Delta x^2 cos2\phi \rangle_{\hat{u}(0)=\hat{e}_x}$ and $\langle \Delta y^2 cos2\phi \rangle_{\hat{u}(0)=\hat{e}_x}$ shown by open symbols in Fig. 4d, which agree well with numerical result of MC simulation. We note that this apparent correlation is different from a true cross-coupling of rotational and translational diffusion, which is only manifested with chiral tracers.

Unlike viscous fluids, for viscoelastic materials such as PEO solution the mobility tensor of the GNR is a function of both lag time and the orientation [45], altering the form of the anisotropic-to-isotropic crossover. We extended our model to an arbitrary non-chiral particle in a linear viscoelastic material [45]. As before, we decomposed the MSDs in x and y directions with initial orientation of $\hat{u}(0) = \hat{e}_x$, for GNRs in viscoelastic PEO solutions, symbols in Fig. 4e. Since the diffusion coefficient is not a constant, we normalized the anisotropic MSDs by their azimuthally averaged values as a function of lag time. To model this data, we used the creep compliance, J, of the solution calculated from nanorheology data via
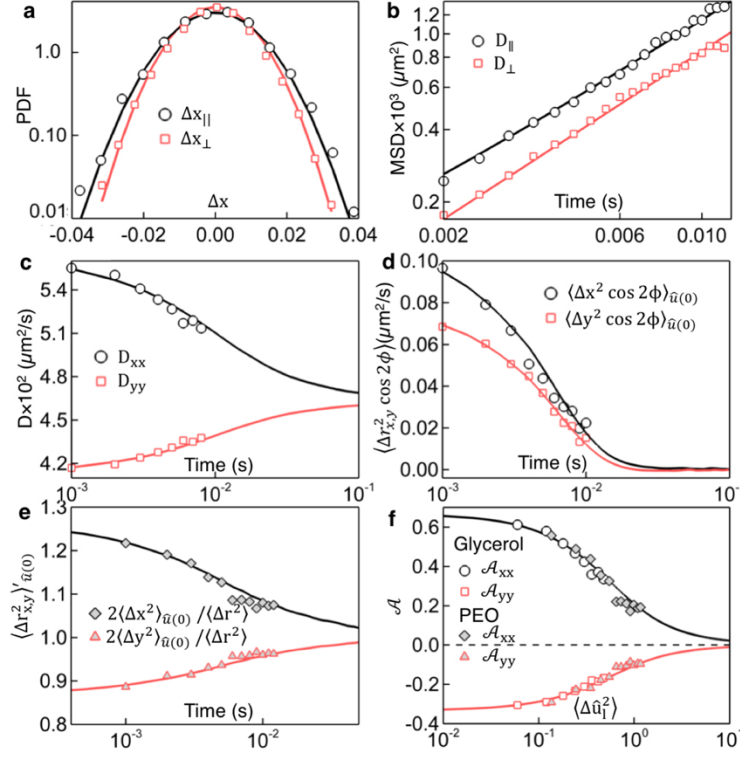
FIG. 4. Anisotropic translational displacement distributions (a), at τ=2 ms, of a GNR in 90% glycerol (symbols) with Gaussian fit (lines) and corresponding anisotropic MSDs (b). Diffusion coefficients of the GNR, (c) corresponding to the data in (a-b), in the fixed lab frame with x-axis aligned with the rod's initial position with model fit, Eq. 3. Mixed translational and orientational correlations (d) in fixed frame (symbols) and MC simulation (curves). Rescaled anisotropic MSDs (e) of GNR in PEO 6.7% (as in Fig. 3e) in the fixed lab frame (symbols) with viscoelastic model (curves); unscaled MSDs shown in Fig. S14 [45]. Diffusion anisotropy (f), , for GNR in glycerol and 6.7% PEO solution (symbols), with model, Eq. 3, (curves).

. While our general model, solid lines in Fig. 4e, matches quantitatively with the current measurement, approximations in our approach will fail in the limit of very soft, predominantly elastic materials [45]. Equation 3 and Fig. 4c and 4e indicate that the rotational diffusion of the GNR controls the rate of the anisotropic-to-isotropic crossover. Therefore, intuitively, one should expect a universal curve for the crossover when plotted against the orientational displacement instead of time. Fig. 4f shows such as rescaled diffusion anisotropy defined as —— based on MSAD for the GNR in both glycerol and PEO solutions. The data for both glycerol, open symbols, and PEO, solid symbols, collapse upon each other and the theoretical model

$131 - \exp{-3} \quad 23 \quad ( )2$, plotted by solid lines.

10

Here we have demonstrated that tracking the rotational Brownian motion of nanorods expands the capabilities of passive microrheology to much smaller length scales and stiffer materials. Moreover, particle heating limits allow much stronger laser illumination than we use here, suggesting that smaller GNRs, stiffer materials and higher frequencies should be accessible. We can imagine mapping out structure and rheology at the 100 nm scale, resolving a typical bacterium into thousands of sub-volumes. The small size of GNRs will also allow the probing of many interfacial systems and soft materials at or near their intrinsic lengthscales, such as many semiflexible polymer materials at their mesh size, or lipid bilayers at the lengthscale of their thermal undulations. This approach promises access to nanoscale structure, dynamics and mechanics in a wide variety of biophysical and soft material systems that are currently accessible, if at all, only to state of the art inelastic neutron or dynamics X-ray scattering methods.

AUTHOR INFORMATION

Corresponding Author

*E-mail: jcrocker@seas.upenn.edu

REFERENCES

[1]   B. R. Dasgupta, S.-Y. Tee, J. C. Crocker, B. Frisken, and D. Weitz, Phys. Rev. E **65**, 051505 (2002).
[2]   T. G. Mason, Rheologica acta **39**, 371 (2000).
[3]   T. Mason, K. Ganesan, J. Van Zanten, D. Wirtz, and S. C. Kuo, Physical Review Letters **79**, 3282 (1997).
[4]   T. G. Mason and D. Weitz, Phys. Rev. Lett. **74**, 1250 (1995).
[5]   D. Chen, E. Weeks, J. C. Crocker, M. Islam, R. Verma, J. Gruber, A. Levine, T. C. Lubensky, and A. Yodh, Physical review letters **90**, 108301 (2003).
[6]   J. C. Crocker, M. T. Valentine, E. R. Weeks, T. Gisler, P. D. Kaplan, A. G. Yodh, and D. A. Weitz, Physical Review Letters **85**, 888 (2000).
[7]   M. Gardel, M. Valentine, J. C. Crocker, A. Bausch, and D. Weitz, Physical review letters **91**, 158302 (2003).
[8]   A. W. Lau, B. D. Hoffman, A. Davies, J. C. Crocker, and T. C. Lubensky, Physical review letters **91**, 198101 (2003).
[9]   K. He, F. Babaye Khorasani, S. T. Retterer, D. K. Thomas, J. C. Conrad, and R. Krishnamoorti, ACS nano **7**, 5122 (2013).
[10]   T. M. Squires and T. G. Mason, Annual Review of Fluid Mechanics **42**, 413 (2010).
[11]   Z. Cheng and T. Mason, Phys. Rev. Lett. **90**, 018304 (2003).
[12]   E. Andablo-Reyes, P. Díaz-Leyva, and J. L. Arauz-Lara, Phys. Rev. Lett. **94**, 106001 (2005).
[13]   C. Haro-Pérez, E. Andablo-Reyes, P. Díaz-Leyva, and J. L. Arauz-Lara, Physical Review E **75**, 041505 (2007).
[14]   F. C. Cheong and D. G. Grier, Opt. Express **18**, 6555 (2010).
[15]   K. V. Edmond, M. T. Elsesser, G. L. Hunter, D. J. Pine, and E. R. Weeks, Proc. Natl. Acad. Sci. **109**, 17891 (2012).

[16]   G. L. Hunter, K. V. Edmond, M. T. Elsesser, and E. R. Weeks, Opt. Express **19**, 17189 (2011).
[17]   D. Mukhija and M. J. Solomon, Journal of colloid and interface science **314**, 98 (2007).
[18]   A. Wang, T. G. Dimiduk, J. Fung, S. Razavi, I. Kretzschmar, K. Chaudhary, and V. N. Manoharan, Journal of Quantitative Spectroscopy and Radiative Transfer **146**, 499 (2014).
[19]   X. Cheng, X. Cao, B. Xiong, Y. He, and E. S. Yeung, Nano Research **10**, 1423 (2017).
[20]   K. Marchuk and N. Fang, Nano lett. **13**, 5414 (2013).
[21]   K. Marchuk, J. W. Ha, and N. Fang, Nano Lett. **13**, 1245 (2013).
[22]   C. Sönnichsen and A. P. Alivisatos, Nano Lett. **5**, 301 (2005).
[23]   E. J. Titus and K. A. Willets, ACS Nano **7**, 6258 (2013).
[24]   G. Wang, W. Sun, Y. Luo, and N. Fang, J. Am. Chem. Soc. **132**, 16417 (2010).
[25]   A. J. Wilson and K. A. Willets, Wiley Interdiscip. Rev.: Nanomed. and Nanobiotech. **5**, 180 (2013).
[26]   L. Xiao, Y. Qiao, Y. He, and E. S. Yeung, Anal. Chem. **82**, 5268 (2010).
[27]   L. Xiao, Y. Qiao, Y. He, and E. S. Yeung, J. Am. Chem. Soc.   **133**, 10638 (2011).
[28]   L. Xiao, L. Wei, C. Liu, Y. He, and E. S. Yeung, Angew. Chem. Int. Ed. **51**, 4181 (2012).
[29]   L. Xiao and E. S. Yeung, Annu. Rev. Anal. Chem. **7**, 89 (2014).
[30]   D. Xu, Y. He, and E. S. Yeung, Anal. Chem. **86**, 3397 (2014).
[31]   H. Yuan, S. Khatua, P. Zijlstra, and M. Orrit, Faraday discussions **167**, 515 (2013).
[32]   S. Alam and A. Mukhopadhyay, Macromolecules **47**, 6919 (2014).
[33]   S. Alam and A. Mukhopadhyay, Langmuir **31**, 8780 (2015).
[34]   R. K. Chhetri, R. L. Blackmon, W.-C. Wu, D. B. Hill, B. Button, P. Casbas-Hernandez, M. A. Troester, J. B. Tracy, and A. L. Oldenburg, Proc. Natl. Acad. Sci. **111**, E4289 (2014).
[35]   R. K. Chhetri, K. A. Kozek, A. C. Johnston-Peck, J. B. Tracy, and A. L. Oldenburg, Phys. Rev. E. **83**, 040903 (2011).
[36]   R. K. Chhetri and A. L. Oldenburg, in *Frontiers in Optics* (Optical Society of America, 2012), p. FTu4E. 3.
[37]   Y. Han, A. M. Alsayed, M. Nobili, J. Zhang, T. C. Lubensky, and A. G. Yodh, Science **314**, 626 (2006).
[38]   F. Perrin, Journal de Physique et le Radium **7**, 1 (1936).
[39]   S. Link and M. A. El-Sayed, (American Chemical Society, 1999).
[40]   C. F. Bohren and D. R. Huffman, Absorption and Scattering of Light by Small Particles, 82 (1983).
[41]   A. Brioude, X. Jiang, and M. Pileni, The Journal of Physical Chemistry B **109**, 13138 (2005).
[42]   P. K. Jain, S. Eustis, and M. A. El-Sayed, The Journal of Physical Chemistry B **110**, 18243 (2006).
[43]   E. M. Purcell and C. R. Pennypacker, The Astrophysical Journal **186**, 705 (1973).
[44]   M. A. Yurkin and A. G. Hoekstra, Journal of Quantitative Spectroscopy and Radiative Transfer **112**, 2234 (2011).
[45]   See Supplemental Material for additional details about the experimental setup, sample prepartion, simulations and derivation which includes Refs. [46-52]
[46]   D. Axelrod, Biophys. J. **26**, 557 (1979).
[47]   H. J. Chen, L. Shao, Q. Li, and J. F. Wang, Chem. Soc. Rev. **42**, 2679 (2013).
[48]   P. B. Johnson and R. W. Christy, Phys. Rev. B **6**, 4370 (1972).

[49]   M. Khan and T. G. Mason, Soft Matter **10**, 9073 (2014).
[50]   M. Khan and T. G. Mason, Phys. Rev. E **89**, 042309 (2014).
[51]   I. Teraoka, *Frontmatter and Index* (Wiley Online Library, 2002).
[52]   M. Rubinstein and R. H. Colby, *Polymer physics* (Oxford University Press New York, 2003), Vol. 23.
[53]   J. C. Crocker and D. G. Grier, J. Colloid Interface Sci. **179**, 298 (1996).
[54]   T. Savin and P. S. Doyle, Biophys. J. **88**, 623 (2005).
[55]   I. Martchenko, H. Dietsch, C. Moitzi, and P. Schurtenberger, J. Phys. Chem. B **115**, 14838 (2011).
[56]   M. M. Tirado, C. L. Martínez, and J. G. de la Torre, The Journal of chemical physics **81**, 2047 (1984).
[57]   A. J. Levine and T. Lubensky, Physical review letters **85**, 1774 (2000).
[58]   L.-H. Cai, S. Panyukov, and M. Rubinstein, Macromolecules **44**, 7853 (2011).
[59]   Y. Cheng, R. K. Prud'Homme, and J. L. Thomas, Macromolecules **35**, 8111 (2002).
[60]   I. Kohli and A. Mukhopadhyay, Macromolecules **45**, 6143 (2012).
[61]   R. Poling-Skutvik, R. Krishnamoorti, and J. C. Conrad, ACS Macro Letters **4**, 1169 (2015).